GEOPHYSICS, VOL. 79, NO. 5 (SEPTEMBER-OCTOBER 2014); P. C123–C134, 6 FIGS.
10.1190/GEO2013-0396.1

Fresnel volume and interface Fresnel zone for reflected and transmitted waves from a curved interface in anisotropic media

Bjørn Ursin[1], Nathalie Favretto-Cristini[2], and Paul Cristini[2]

ABSTRACT

The Fresnel volume and the interface Fresnel zone (IFZ) concepts play an important role in seismic exploration because the IFZ largely contributes to the formation of the reflection and transmission wavefields at an observation point. We derived analytic expressions based on traveltime approximations to evaluate the IFZ size for converted and nonconverted waves reflected (or transmitted) by a curved interface between two homogeneous general anisotropic media, and more specifically for dip-constrained transversely isotropic homogeneous media. The reflectors are of anticline, syncline, or saddle type, and their principal curvature axes may not lie in the incidence plane. As in an anisotropic medium the isochron in most cases assumes a nonelliptical shape, the size and the shape of the IFZ for reflected waves are predominantly dependent on the curvatures of the isochrons together with the curvatures of the interface. The IFZ shapes also exhibit large variation with interface curvature and incidence angle. In addition, the difference between the Thomsen anisotropy parameters ϵ and δ is found to control the size of the IFZ for P-P and P-S reflections. The IFZ for anisotropic media with curved interface can be much larger than that for equivalent isotropic media, and more specifically for positive values of $\epsilon - \delta$. The spatial resolution of unmigrated seismic data in anisotropic media would consequently be different from that determined for the same configuration for isotropic models and a planar interface.

INTRODUCTION

The Fresnel volume (FV) concept (Kravtsov and Orlov, 1990) plays an important role in the formation of the seismic field at an observation point. Of particular interest for seismic exploration is the size of the interface Fresnel zone (IFZ), i.e., the intersection of the FV with an interface. This finite area of a reflector can be viewed as the region of constructive reflection interference surrounding the reflection point of the geometrical ray. The IFZ determines the spatial resolving power for unmigrated seismic data with which important lithological changes along a seismic profile direction may be observed (Sheriff, 1980). Additionally, it also largely contributes to the reflected and transmitted wavefields, and more specifically to their amplitude (Spetzler and Snieder, 2004; Favretto-Cristini al., 2007a, 2007b). As a consequence, the IFZ has received increasing attention in past decades.

Analytic and numerical modeling techniques have been used to determine the IFZ dimensions in various configurations. Hubral and his coworkers define the projected Fresnel zone of a zero-offset reflection onto the subsurface reflector using a standard 3D CMP traveltime analysis, without knowing the overburden (Hubral et al., 1993; Schleicher et al., 1997). Červený (2001) suggests two methods that include FV parameter calculations into the ray tracing procedure in complex 2D and 3D structures. The first one, called FV ray tracing (Červený and Soares, 1992), combines paraxial ray approximation with dynamic ray tracing and is only applicable to zero-order waves (i.e., direct, reflected, and transmitted waves...), whereas the second, more accurate, method is based on network ray tracing (Kvasnička and Červený, 1994). Unfortunately, it can be applied only to first arrivals at receivers. Moser and Červený (2007) show how the Fresnel region can be calculated by conventional dynamic ray tracing in Cartesian coordinates, for isotropic and anisotropic inhomogeneous layered media. However, the derivations are cumbersome. Pulliam and Snieder (1998) outline an efficient scheme based on ray perturbation theory to compute approximate FZs in inhomogeneous media.

Manuscript received by the Editor 25 October 2013; revised manuscript received 18 March 2014; published online 21 July 2014.
[1]Norwegian University of Science and Technology (NTNU), Department of Petroleum Engineering and Applied Geophysics, Trondheim, Norway. E-mail: bjorn.ursin@ntnu.no.
[2]LMA, CNRS, UPR 7051, Aix-Marseille University, Centrale Marseille, Marseille, France. E-mail: favretto@lma.cnrs-mrs.fr; cristini@lma.cnrs-mrs.fr.

With the help of the Kirchhoff approximation and on the basis of the reciprocity relation, Gelchinsky (1985) derives symmetrized invariant formulas for the computation of IFZ and FV for structurally complex media (e.g., an inhomogeneous medium with curved interfaces), the limitation being that the medium is considered locally homogeneous in the vicinity of the FZ center. Kvasnička and Červený (1996a, 1996b) derive analytical expressions for FVs of seismic body waves and for IFZ for simple structures with plane interfaces, which offer a deeper insight into the properties of the FV and IFZ. It is interesting to note that FV boundaries with corresponding FZ can also be estimated using the method of isochron rays (Iversen, 2004, 2006). Monk (2010) examines the shape of the IFZ for nonzero offset and in the situation of a constant velocity gradient, using a derivation that takes a largely geometric approach. Eaton et al. (1991) derive formulas for the P-SV Fresnel-zone radius for surface and VSP geometries. Lindsey (1989) empirically studies the changes in IFZ size for normal wave incidence when the reflector is either a syncline or an anticline, as compared with the IFZ size for a plane reflector. Favretto-Cristini et al. (2009) extend the study of Lindsey to the case of oblique wave incidence onto a spherically shaped interface of anticline or syncline type by deriving analytical expressions for the size of the IFZ.

Most studies are concerned with zero-offset configurations and plane reflectors. In addition, few works have been devoted to anisotropic media. For instance, Okoye and Uren (2000) calculate the FZ diameter for zero-offset configurations for P- and SH-waves in TI media and isotropic media and for dipping plane reflectors. They conclude that the FZ diameter is predominantly dependent on the curvatures and wavelength of the wavefront as well as the dip angle of the reflector. The parameter δ^* and the Thomsen anisotropy parameters ϵ and γ also affect the FZ diameter.

The purpose of the paper is to address the issue of deriving simple analytical expressions for the IFZ for multioffset configurations and a curved interface between anisotropic media. More specifically, we propose to generalize the work reported in Favretto-Cristini et al. (2009) for the IFZ for (possibly converted) reflected and transmitted waves from a nonspherically shaped interface between anisotropic media. Indeed, in Favretto-Cristini et al. (2009), the analytic derivations take a geometric approach based on analytical expressions of shifted isochrons (which are of a simple form for isotropic media), and they can hardly be extended to the case of more complex media (e.g., anisotropic media) without numerical developments. Analytical expressions, even approximate, could, however, provide valuable insight into the influence of anisotropic parameter combinations on the shape and size of the IFZ and hence on the horizontal seismic resolution. This is the objective of this paper.

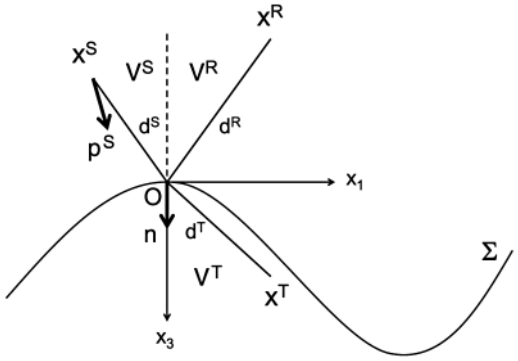

Figure 1. Incident S, reflected R, and transmitted T waves at a curved interface Σ between two anisotropic media. The slowness and group velocity vectors are denoted by $\mathbf{p}$ and $\mathbf{V}$, respectively. The source (respectively, the receiver) is located at $\mathbf{x}^{\mathbf{S}}$ (respectively, $\mathbf{x}^{\mathbf{R},\mathbf{T}}$) at a distance d^S (respectively, $d^{R,T}$) from the reflection/transmission point O.

The organization of the paper is as follows. The second section reviews some basic concepts of wave propagation in anisotropic media and establishes analytical expressions for the IFZ for reflected and transmitted waves from a curved interface between two anisotropic media. The third section considers the particular case of dip-constrained transversely isotropic (DTI) media (Ayzenberg et al., 2009; Farra and Pšenčík, 2013), i.e., TI media with the symmetry axis orthogonal to the curved reflector at each point of the interface. The weak-anisotropy approximation (Thomsen, 1986) has proved extremely useful in identifying anisotropy parameter combinations responsible for various seismic signatures (Tsvankin, 2001; Tsvankin and Grechka, 2011). It is used here to gain valuable analytic insight into the influence of certain anisotropy parameters on the size of the IFZ. The formulae for isotropic media are presented in the fourth section. The last section investigates the shape and the size of the IFZ for P-P and P-SV reflections as a function of anisotropy parameters for various incidence angles and interface curvatures. Results obtained indicate that, in addition to the curvature of the interface (of anticline, syncline, or saddle type), a certain combination of the anisotropy parameters controls the IFZ shape and size and hence the horizontal seismic resolution.

ANISOTROPIC MEDIA

We consider a curved interface between two homogeneous anisotropic media. An incident wave strikes the interface and gives rise to reflected and transmitted waves. These waves may be of arbitrary types. We choose the coordinate system with the origin at the reflection/transmission point. The normal to the interface points into the medium of the transmitted waves. The x_1-axis lies in the surface tangent plane and in the plane defined by the surface normal and the slowness of the incident wave, and the x_3-axis is parallel to the surface normal (Figure 1).

The slownesses of the incident, reflected and transmitted waves ($\mathbf{p}^{\mathbf{S}}$, $\mathbf{p}^{\mathbf{R}}$, $\mathbf{p}^{\mathbf{T}}$, respectively) lie then all in the $x_1 - x_3$ plane, i.e., the plane of incidence. This implies that the out-of-plane components $p_2^U (U = S, R, T)$ of these slowness vectors are equal to zero. The superscript S denotes the quantities for the incident wave, R for the reflected wave, and T for the transmitted wave.

We consider that the source is located at $\mathbf{x}^{\mathbf{S}} = (x_1^S, x_2^S, x_3^S)$ at a distance

$$d^S = \|\mathbf{x}^{\mathbf{S}}\| = [(x_1^S)^2 + (x_2^S)^2 + (x_3^S)^2]^{\frac{1}{2}} \qquad (1)$$

from the reflection/transmission point O. The receiver point can be located either in the incident medium or in the transmitted medium at $\mathbf{x}^{\mathbf{R},\mathbf{T}} = (x_1^{R,T}, x_2^{R,T}, x_3^{R,T})$ at a distance $d^{R,T}$ from the reflection/transmission point O.

Traveltime approximations

The difference in traveltime between a ray from point $\mathbf{x}$ to the origin O and from point $\mathbf{x}$ to a point at $\delta\mathbf{x}$ near the origin O is

$$\delta T(\mathbf{x},\delta\mathbf{x}) = T(\mathbf{x},\delta\mathbf{x}) - T(\mathbf{x},0) = \frac{1}{V+\delta V}\|x-\delta\mathbf{x}\| - \frac{1}{V}\|\mathbf{x}\|, \quad (2)$$

where V is the group velocity,

$$V = \|\mathbf{V}\| = (V_1^2 + V_2^2 + V_3^2)^{\frac{1}{2}}, \quad (3)$$

and δV is the change in group velocity for the perturbed ray. With $d = \|\mathbf{x}\|$, we obtain the approximation

$$\delta T(\mathbf{x},\delta\mathbf{x}) \simeq \frac{d}{V}\left[\left(1-\frac{\delta V}{V}\right)\left(1-2\frac{\mathbf{x}\cdot\delta\mathbf{x}}{d^2}+\frac{\|\delta\mathbf{x}\|^2}{d^2}\right)^{\frac{1}{2}}-1\right]. \quad (4)$$

Expanding the square-root term in a Taylor series and considering $(\frac{\|\delta\mathbf{x}\|}{d})^3 \ll 1$ leads to a second-order approximation for the traveltime difference:

$$\delta T(\mathbf{x},\delta\mathbf{x}) \simeq \frac{1}{2Vd}\left(1-\frac{\delta V}{V}\right) \times \left[\|\delta\mathbf{x}\|^2 - 2\mathbf{x}\cdot\delta\mathbf{x} - \left(\frac{x\cdot\delta\mathbf{x}}{d}\right)^2\right] - \frac{\delta V}{V^2}. \quad (5)$$

Neglecting changes in group velocity V (i.e., $\frac{\delta V}{V} \ll 1$) leads to a small relative error in the traveltime difference and

$$\delta T(\mathbf{x},\delta\mathbf{x}) \simeq \frac{1}{2Vd}\left[\|\delta\mathbf{x}\|^2 - 2\mathbf{x}\cdot\delta\mathbf{x} - \left(\frac{x\cdot\delta\mathbf{x}}{d}\right)^2\right]. \quad (6)$$

Let the group velocity vector $\mathbf{V}$ point away from the origin O, so that

$$\mathbf{x} = \frac{d}{V}\mathbf{V}. \quad (7)$$

The approximate traveltime difference may then be expressed as a function of the group velocity:

$$\delta T(\mathbf{V},\delta\mathbf{x}) \simeq \frac{1}{2Vd}\left[\|\delta\mathbf{x}\|^2 - 2d\frac{\mathbf{V}\cdot\delta\mathbf{x}}{V} - \left(\frac{\mathbf{V}\cdot\delta\mathbf{x}}{V}\right)^2\right]. \quad (8)$$

Fresnel volumes and interface Fresnel zones

The FVs associated with the reflected or transmitted wave are defined by

$$|\delta T(\mathbf{x}^{\mathbf{S}},\delta\mathbf{x}) + \delta T(\mathbf{x}^{\mathbf{U}},\delta\mathbf{x})| \le \frac{1}{2f} \quad (U=R,T) \quad (9)$$

or

$$|\delta T(\mathbf{V}^{\mathbf{S}},\delta\mathbf{x}) + \delta T(\mathbf{V}^{\mathbf{U}},\delta\mathbf{x})| \le \frac{1}{2f} \quad (U=R,T), \quad (10)$$

where f is the dominant frequency of the signal and δT has to be replaced with its approximation 6 or 8 with the appropriate superscript.

The wave is reflected or transmitted at a curved interface Σ, which may locally be approximated by a second-order expression:

$$x_3 = F(x_1,x_2) = \frac{1}{2}(x_1,x_2)\mathbf{F}(x_1,x_2)^t = \frac{1}{2}(F_{11}x_1^2 + 2F_{12}x_1x_2 + F_{22}x_2^2). \quad (11)$$

Equation 9 for the reflected wave is valid only for $\delta x_3 \le F(\delta x_1,\delta x_2)$, and for the transmitted wave, it is valid only for $\delta x_3 \ge F(\delta x_1,\delta x_2)$. For Fresnel zones at the curved interface, we have $\delta x_3 = F(\delta x_1,\delta x_2)$.

Using expression 11 in equation 6 and only keeping terms up to second-order leads to the approximation for the traveltime difference:

$$\delta T_\Sigma(\mathbf{x},\delta x_1,\delta x_2) \simeq \frac{1}{2Vd}\left[\left(1-\frac{x_1^2}{d^2}\right)\delta x_1^2 + \left(1-\frac{x_2^2}{d^2}\right)\delta x_2^2 - 2\frac{x_1x_2}{d^2}\delta x_1\delta x_2 - 2x_1\delta x_1 - 2x_2\delta x_2 - 2F(\delta x_1,\delta x_2)x_3\right] \quad (12)$$

or

$$\delta T_\Sigma(\mathbf{V},\delta x_1,\delta x_2) \simeq \frac{1}{2Vd}\left[\left(1-\frac{V_1^2}{V^2}\right)\delta x_1^2 + \left(1-\frac{V_2^2}{V^2}\right)\delta x_2^2 - 2\frac{V_1V_2}{V^2}\delta x_1\delta x_2\right] - \frac{V_1}{V^2}\delta x_1 - \frac{V_2}{V^2}\delta x_2 - F(\delta x_1,\delta x_2)\frac{V_3}{V^2}. \quad (13)$$

The IFZs for the reflected and transmitted waves are then defined as the points on the interface that satisfy the inequality

$$|\delta T_\Sigma(\mathbf{x}^{\mathbf{S}},\delta x_1,\delta x_2) + \delta T_\Sigma(\mathbf{x}^{\mathbf{U}},\delta x_1,\delta x_2)| \le \frac{1}{2f} \quad (U=R,T) \quad (14)$$

or

$$|\delta T_\Sigma(\mathbf{V}^{\mathbf{S}},\delta x_1,\delta x_2) + \delta T_\Sigma(\mathbf{V}^{\mathbf{U}},\delta x_1,\delta x_2)| \le \frac{1}{2f} \quad (U=R,T), \quad (15)$$

in which δT_Σ has to be substituted by its expression 12 or 13 with the appropriate superscript.

In our situation, the position vector $\mathbf{x}^{\mathbf{S}}$ of the source point and the slowness vector $\mathbf{p}^{\mathbf{S}}$ are given. From the group velocity vector $\mathbf{V}^{\mathbf{S}}$, we determine the reflection/transmission point. By virtue of Snell's law, the horizontal slowness p_1, determined from the slowness vector and the surface tangent, is constant for all waves. Because the out-of-plane component of the slowness vector is equal to zero for all waves, the vertical slowness $p_3^U(U=R,T)$ is thus computed using equation A-3 with the proper wave type and by applying a

proper radiation condition. The group velocity vector $\mathbf{V}^{\mathbf{U}}(U = R, T)$ is then computed using the results in Appendix A with the correct medium parameters, proper wave mode, and considering $\mathbf{p} = (p_1, 0, p_3)$. The receiver points for the reflected and transmitted rays are finally computed from equation 7 when the lengths of the respective rays are given (Figure 1).

DIP-CONSTRAINED TRANSVERSELY ISOTROPIC MEDIA

To provide analytic insight into the influence of anisotropy on the IFZ, we apply the previous theory to a curved interface between two DTI media (Ayzenberg et al., 2009; Farra and Pšenčík, 2013). The symmetry axis of both media is then parallel to the interface normal at each point of the interface. At the reflection point, both half-spaces are VTI in the local coordinate system because the symmetry axis is parallel to the x_3-axis. The three wave types that may occur are the SH-wave and coupled P-SV-waves. Because of the symmetry, all seismic signatures depend only on the angle between the propagation direction and the symmetry axis. The out-of-plane components of the group velocity vector and slowness vector are equal to zero in all cases. From equation 7, x_2 is equal to zero as well. Consequently, expression 13 for the traveltime difference becomes

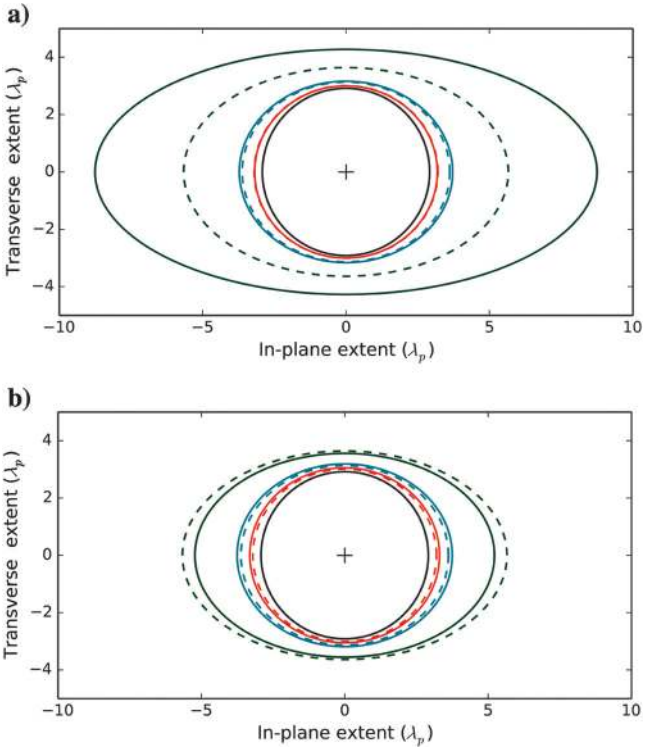

Figure 2. Variation in the shape and size of the IFZ for P-P reflection from a plane reflector between anisotropic (solid line) and isotropic (dashed line) media, as a function of the difference $\epsilon - \delta$ (with a positive [top] or negative [bottom] value) and for various incidence angles θ. The incidence angles are $\theta = 0^\circ$ (black), $\theta = 20^\circ$ (red), $\theta = 30^\circ$ (light blue), and $\theta = 50^\circ$ (green). The size of each IFZ is normalized with respect to the incident P-wavelength for $\theta = 0^\circ$.

$$\delta T_\Sigma(\mathbf{V}, \delta x_1, \delta x_2) \simeq \frac{1}{2Vd}\left[\left(1 - \frac{V_1^2}{V^2}\right)\delta x_1^2 + \delta x_2^2\right] - \frac{V_1}{V^2}\delta x_1 - F(\delta x_1, \delta x_2)\frac{V_3}{V^2}. \tag{16}$$

Exact expressions for the group velocities V_1 and V_3 are given in Appendix B. For the SH-wave, the expressions are simple, but for the P- and SV-waves, they are more complicated. Even if it is preferable to use the exact expressions in actual modeling, inversion, and processing algorithms, we shall instead use the approximate dispersion relation to gain analytic insight into the effects of anisotropy on the IFZ. These approximate dispersion relations for P-waves are (Pestana et al., 2012)

$$\omega^2 = v_{P0}^2[(1 + 2\epsilon)k_1^2 + k_3^2] - 2\frac{v_{P0}^2(\epsilon - \delta)k_1^2k_3^2}{k_3^2 + \xi k_1^2}, \tag{17}$$

where $k_1 = \omega p_1$ and $k_3 = \omega p_3$, and for SV-waves,

$$\omega^2 = v_{S0}^2(k_1^2 + k_3^2) + 2\frac{v_{P0}^2(\epsilon - \delta)k_1^2k_3^2}{k_3^2 + \xi k_1^2}, \tag{18}$$

where the notation of Thomsen (1986) is used:

$$\begin{cases} v_{P0} = \sqrt{\frac{c_{33}}{\rho}} \\ v_{S0} = \sqrt{\frac{c_{44}}{\rho}} \\ \epsilon = \frac{c_{11} - c_{33}}{2c_{33}} \\ \delta = \frac{(c_{13} + c_{44})^2 - (c_{33} - c_{44})^2}{2c_{33}(c_{33} - c_{44})} \end{cases}, \tag{19}$$

where v_{P0} and v_{S0} are the vertical velocities defined by the density ρ and the elastic constants c_{ij} given in Voigt notation and

$$\xi = 1 + 2\epsilon\frac{v_{P0}^2}{v_{P0}^2 - v_{S0}^2}. \tag{20}$$

The approximate dispersion relations 17 and 18 are valid for

$$\left|\frac{2(\epsilon - \delta)v_{P0}^2(v_{P0}^2 - v_{S0}^2)\sin^2 2\theta}{[v_{P0}^2(1 + 2\epsilon\sin^2\theta) - v_{S0}^2]^2}\right| \ll 1, \tag{21}$$

with θ being the angle between the slowness vector and the symmetry axis. They provide independent equations for P- and SV-waves. Using equations 17 and 18, together with equation A-7, yields the components of the group velocity for P-waves:

$$\begin{cases} V_{P1} = v_{P0}^2 p_1[(1 + 2\epsilon) - 2(\epsilon - \delta)\chi] \\ V_{P3} = v_{P0}^2 p_3[1 - 2(\epsilon - \delta)\chi'] \end{cases} \tag{22}$$

and for SV-waves:

$$\begin{cases} V_{S1} = v_{S0}^2 p_1[1 + 2\sigma\chi] \\ V_{S3} = v_{S0}^2 p_3[1 + 2\sigma\chi'] \end{cases}, \tag{23}$$

where

$$\begin{cases} \chi = \frac{p_3^4}{(p_3^2+\xi p_1^2)^2} \\ \chi' = \frac{\xi p_1^4}{(p_3^2+\xi p_1^2)^2} \end{cases} \quad (24)$$

and

$$\sigma \equiv \frac{v_{P0}^2}{v_{S0}^2}(\epsilon - \delta). \quad (25)$$

From equations 16 and 22, we can note that the traveltime difference for P-waves is controlled by the interface parameters F, the vertical P-wave velocity v_{P0}, the anisotropy parameter ϵ, and the parameter combination $\epsilon - \delta$. Equations 16 and 23 show that the traveltime difference for SV-waves is controlled by the interface parameters F, the vertical S-wave velocity v_{S0}, and the above-defined parameter σ, which is proportional to the difference $\epsilon - \delta$. Consequently, beside the interface parameters F and the vertical velocities v_{P0} and v_{S0}, the difference $\epsilon - \delta$ also controls the shape and the size of the IFZ for P-P and P-SV reflections.

The IFZ for a P-SV reflected wave in a DTI medium is computed in Appendix C. The IFZ for a P-P reflected wave can be straightforwardly deduced from these derivations.

ISOTROPIC MEDIA

For isotropic media, the previous computations simplify considerably because there are only two parameters: the velocities v_{P0} and v_{S0} of P- and S-waves, respectively. Nevertheless, the general equations 9 and 14 defining the FV and IFZ, respectively, remain the same.

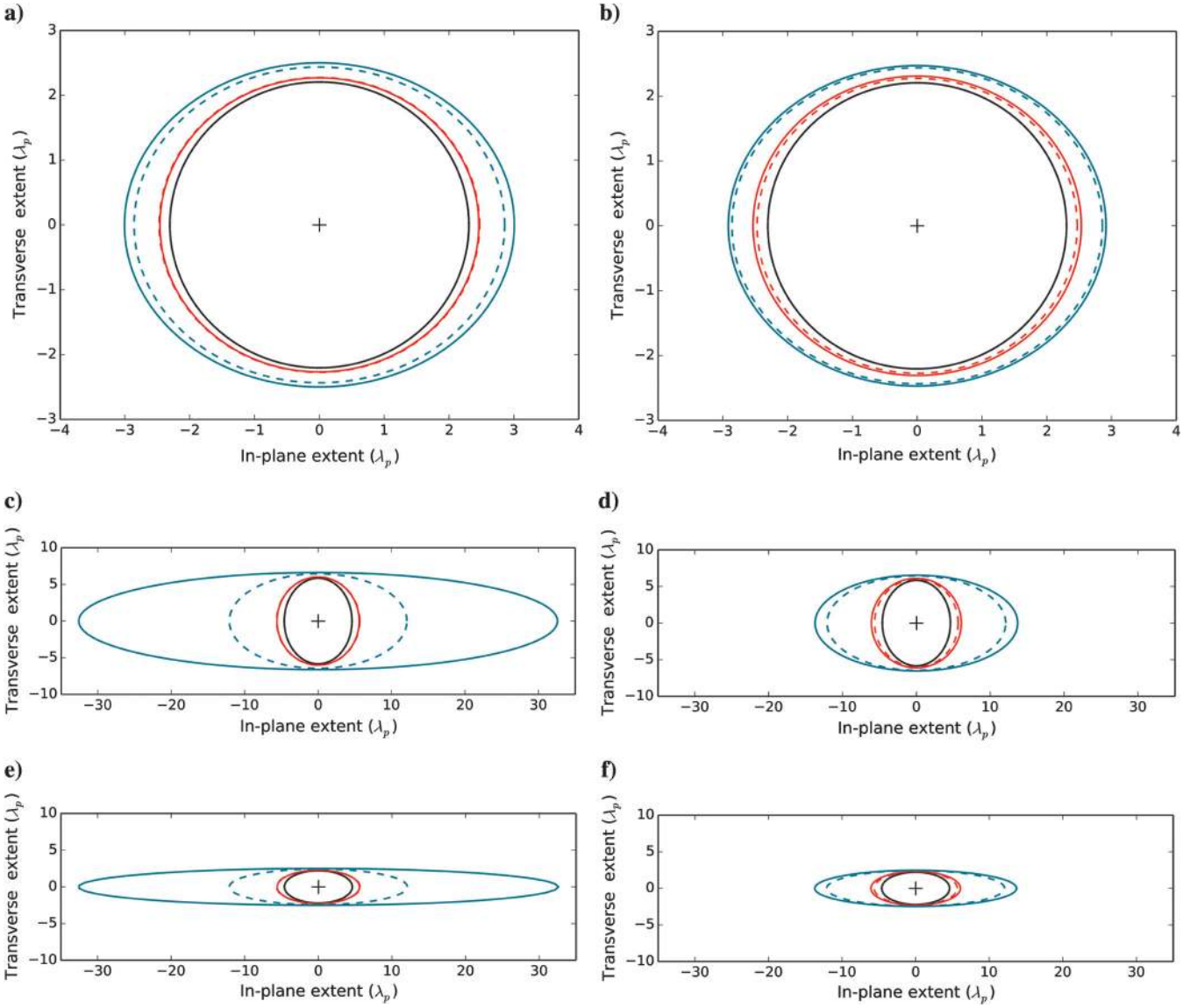

Figure 3. Variation in the shape and size of the IFZ for P-P reflection in anisotropic (solid line) and isotropic (dashed line) media at an anticline- (top), syncline- (middle), and saddle-type (bottom) reflector, as a function of the difference $\epsilon - \delta$ (with positive [left] or negative [right] value) and for various incidence angles θ. The incidence angles are $\theta = 0^\circ$ (black), $\theta = 20^\circ$ (red), and $\theta = 35^\circ$ (light blue). The principal curvature axes of the reflectors lie along the Cartesian coordinate axes. The size of each IFZ is normalized with respect to the incident P-wavelength for $\theta = 0^\circ$.

For an isotropic medium, the IFZ for a P-SV reflected wave is given by equation C-1 taking into account Snell's law:

$$\frac{1}{2v_{P0}d_P}(\cos^2\theta_P\delta x_1^2+\delta x_2^2)+F(\delta x_1,\delta x_2)\left(\frac{\cos\theta_P}{v_{P0}}+\frac{\cos\theta_S}{v_{S0}}\right)+\frac{1}{2v_{S0}d_P}(\cos^2\theta_S\delta x_1^2+\delta x_2^2)\le\frac{1}{2f},\tag{26}$$

where θ_P and θ_S are the angles the rays for the P- and SV-waves make with the surface normal, respectively.

NUMERICAL EXAMPLES

Here, we do not consider transmitted waves and focus only on the reflection at a curved interface between two DTI media. The shape and the size of the IFZ for P-P and P-SV reflections are investigated for various anisotropy parameters, incidence angles, and interface curvatures. The purpose is to demonstrate how all these parameters, and specifically the anisotropy parameters, may control the IFZ size and hence the lateral seismic resolution. To emphasize this influence, we compare the results with those obtained for the equivalent isotropic media and plane reflectors.

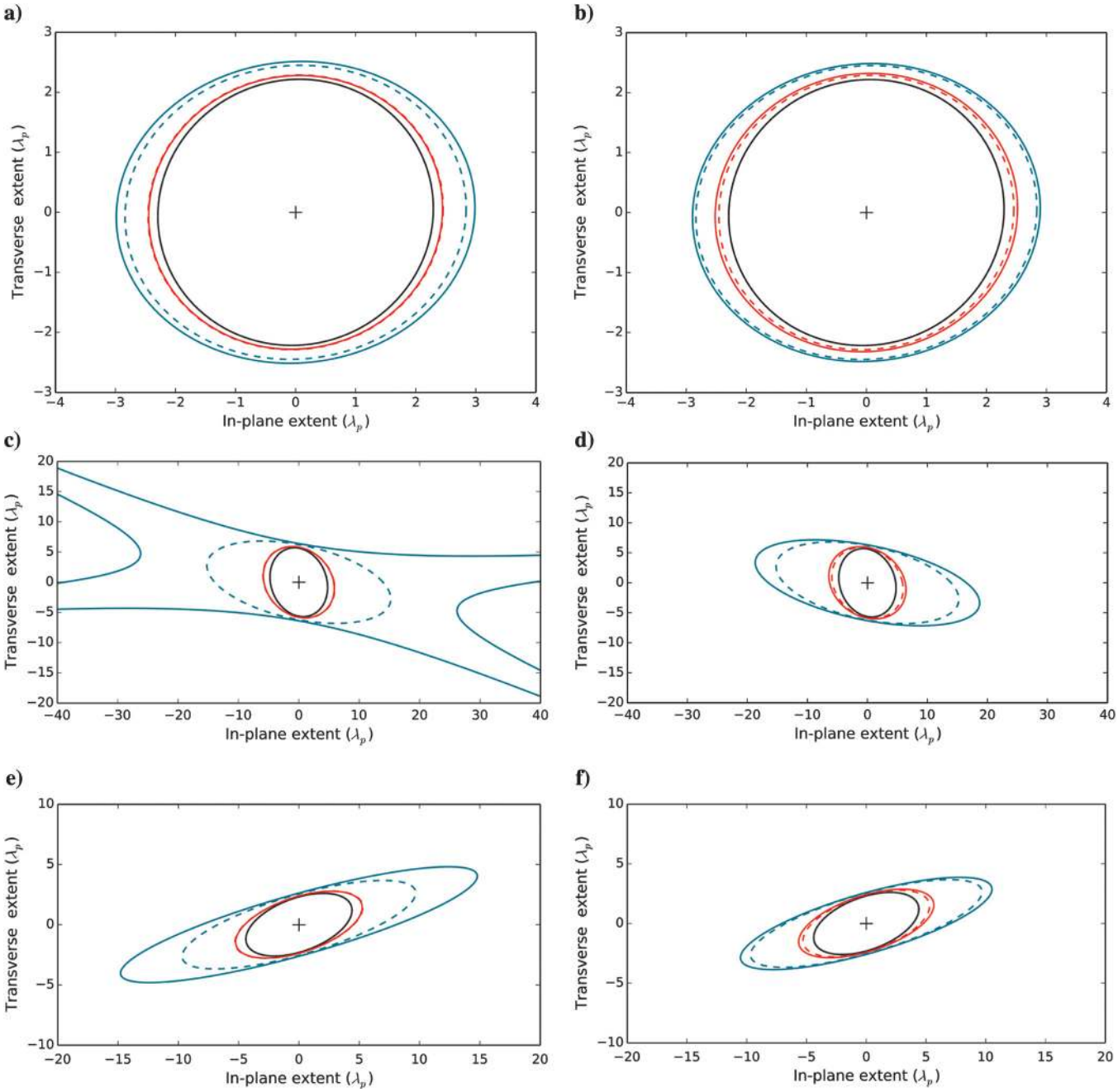

Figure 4. Same as in Figure 3, except that the principal curvature axes of the reflectors do not lie along the Cartesian coordinate axes (rotation of the curvature axes by $\phi = 20^\circ$ with respect to the x_1- and x_2-axes).

Description of the model

We use the measured values of anisotropy parameters in brine-saturated shales (Wang, 2002). The incidence medium has density $\rho = 2597$ kg/m^3, vertical P-wave velocity $v_{P0} = 4409$ m/s, vertical S-wave velocity $v_{S0} = 2688$ m/s, and Thomsen parameters $\epsilon = 0.110$ and $\delta = -0.043$. The velocities and Thomsen parameters are connected to elastic coefficients $a_{ij} = c_{ij}/\rho$ through equation 19. Alkhalifah and Tsvankin (1995) introduce the traveltime parameter $\eta = \frac{\epsilon-\delta}{1+2\delta}$, which appears in the relation between the horizontal velocity and NMO velocity for a P-P reflection in a VTI layer. In the exact expression and in the relations for traveltimes in a layered VTI medium (Ursin and Stovas, 2006), only the difference $\epsilon - \delta$ appears. This is also the case for the dispersion relation for P and SV waves in a VTI medium (Tsvankin, 2001; Pestana et al., 2012). Here, we shall consider this difference, which in the previous sections was found to also control the IFZ size for P-P and P-SV reflections. The difference $\epsilon - \delta$ is positive for most sedimentary rocks, and a typical value is $\epsilon - \delta = 0.153$ for real brine-saturated shales. For comparison purposes, and to emphasize the influence of this difference on the shape and the size of the IFZ, we fix the parameters ρ, v_{P0}, and v_{S0}, and we also consider a negative value for $\epsilon - \delta$ (-0.153). The source and the receiver are located at a distance $x_3 = 3000$ m from the plane tangent to the interface at the reflection point. The central frequency f of the incident P-wave is chosen equal to 25 Hz. The incident P-wavelength at normal incidence is then 176 m.

We consider three kinds of curved reflector in this study: an anticline-type reflector with positive values for the main radii of interface curvature (Ursin, 1986) ($R_1 = +5000$ m and $R_2 = +4000$ m), a syncline-type reflector with negative values for radii ($R_1 = -5000$ m and $R_2 = -4000$ m), and a saddle-type reflector with $R_1 = -5000$ m and $R_2 = +4000$ m. To remain general, we cannot suppose that δx_1 and δx_2 lie along the principal curvature axes of the interface because the x_1-direction is given by the incoming ray, which implies that the functions $F_{ij}(i, j = 1, 2)$ in equation 11 can be expressed as (Stavroudis, 1972, p. 149)

$$\begin{cases} F_{11} = \frac{1}{R_1}\cos^2\phi + \frac{1}{R_2}\sin^2\phi \\ F_{12} = (\frac{1}{R_1} - \frac{1}{R_2})\cos\phi\,\sin\phi\,, \\ F_{22} = \frac{1}{R_1}\sin^2\phi + \frac{1}{R_2}\cos^2\phi \end{cases} \tag{27}$$

where ϕ is the angle between the principal curvature axes of the interface and the Cartesian coordinate axes. Hereafter, we will consider $\phi = 20^\circ$. We also consider the particular case where δx_1 and δx_2 both lie along the principal curvature axes of the interface, which implies $\phi = 0$, and hence

$$\begin{cases} F_{11} = \frac{1}{R_1} \\ F_{12} = 0\,. \\ F_{22} = \frac{1}{R_2} \end{cases} \tag{28}$$

Note that for a plane reflector, the radii R_1 and R_2 have infinite values.

Influence of $\epsilon - \delta$ on the interface Fresnel zone for P-P reflection from various curved reflectors

We first wanted to validate the results provided by our approximation with the results obtained with the method suggested in Favretto-Cristini al. (2009) in the simpler case of a curved interface between isotropic media. More specifically, the variation in the size of the IFZ for a P-P reflection as a function of the incidence angle θ, and for a given value of the radii $R_{1,2}$, was investigated. On the one hand, this variation is obtained using equations 8 and 11 given in Favretto-Cristini et al. (2009), and on the other hand, through equation 26, taking into account the specific alignment given in equation 28. We obtained a very good agreement between the results whatever the interface curvature. For the syncline-type interface, this very good agreement occurs up to the particular incidence angle for which the radius of the interface curvature approaches the radius of curvature of the isochron associated with the specular reflection.

In a second step, we study the effects of the difference $\epsilon - \delta$ on the shape and the size of the IFZ for P-P reflection for various incidence angles and various interface curvatures.

Figure 2 illustrates the results for a plane reflector. For comparison purposes, we also show the IFZs for the equivalent isotropic medium ($\epsilon = \delta = 0$). The size of each IFZ is normalized with respect to the incident P-wavelength for $\theta = 0$. For $\theta = 0$, the anisotropic IFZ is equivalent to the isotropic counterpart and exhibits a circular shape. This result seems to contradict that presented in Okoye and Uren (2000). In fact, our zero-offset results for anisotropic media are due to the traveltime approximation, which consists in an expansion in a Taylor series around the central ray (see equation 5). Because the reflector dip is zero, the zero-offset

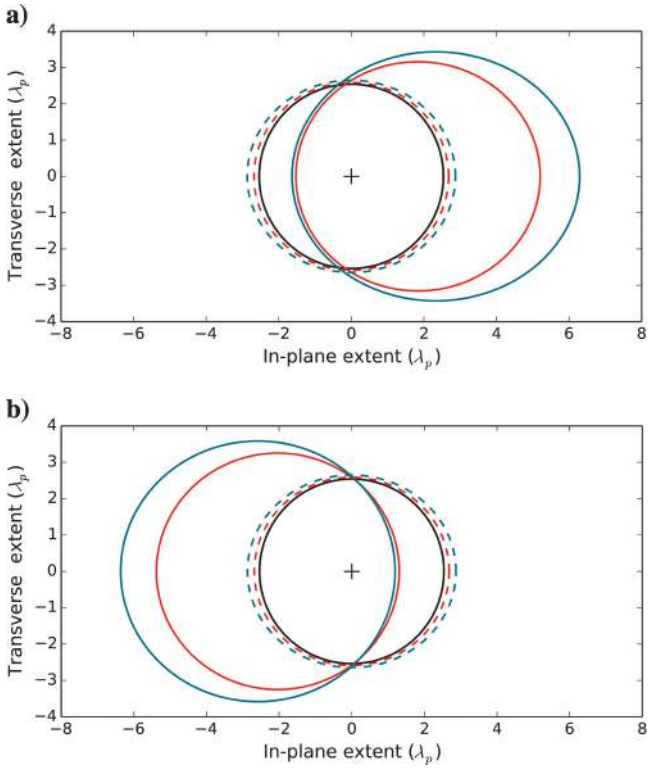

Figure 5. Variation in the shape and size of the IFZ for P-SV reflection from a plane reflector between anisotropic (solid line) and isotropic (dashed line) media, as a function of the difference $\epsilon - \delta$ (with a positive [top] or negative [bottom] value) and for various incidence angles θ. The incidence angles are $\theta = 0^\circ$ (black), $\theta = 20^\circ$ (red), and $\theta = 30^\circ$ (light blue). The size of each IFZ is normalized with respect to the incident P-wavelength for $\theta = 0^\circ$.

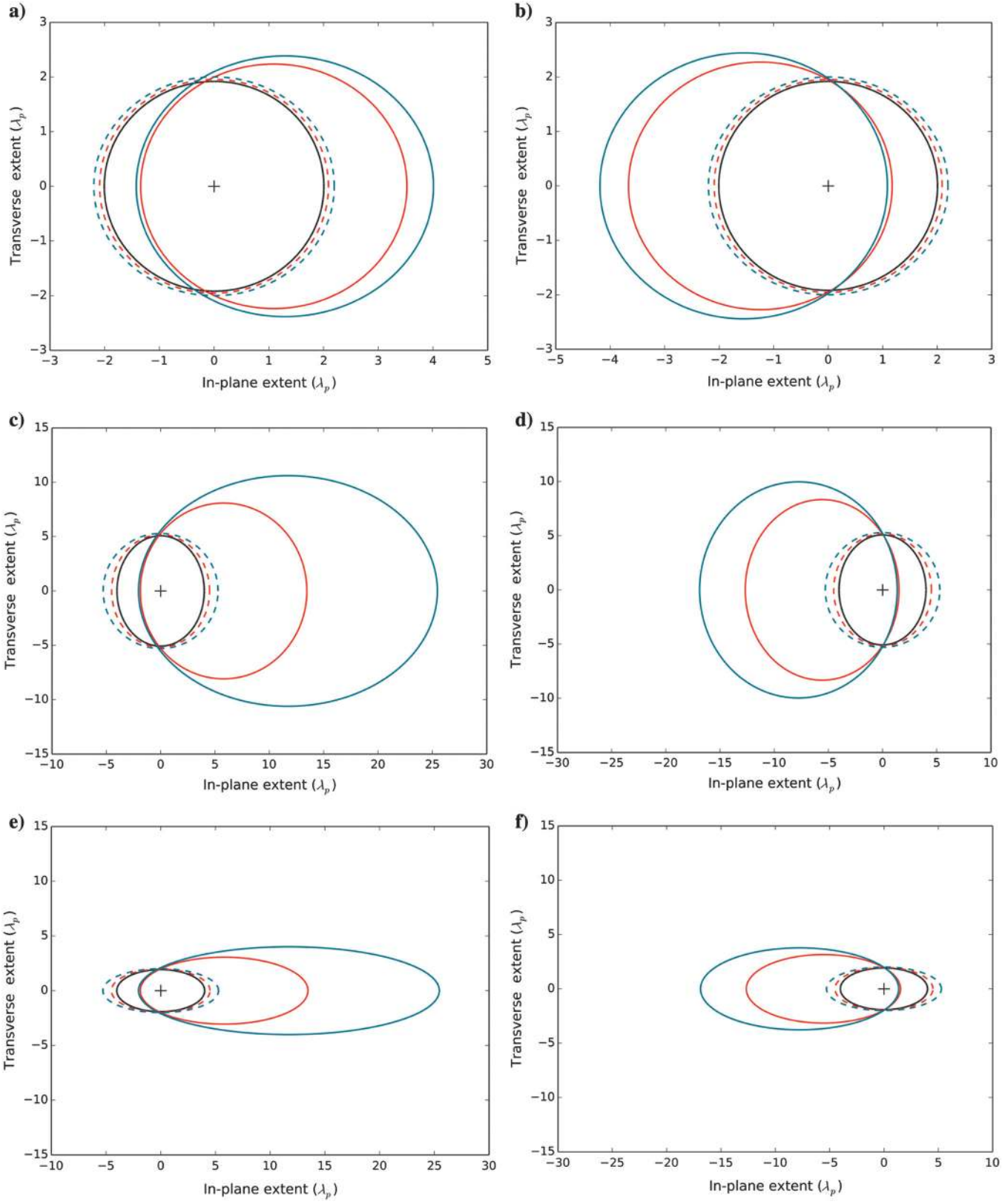

Figure 6. Variation in the shape and size of the IFZ for P-SV reflection in anisotropic (solid line) and isotropic (dashed line) media at an anticline- (top), syncline- (middle), and saddle-type (bottom) reflector, as a function of the difference $\epsilon - \delta$ (with a positive [left] or negative [right] value) and for various incidence angles θ. The incidence angles are $\theta = 0^\circ$ (black), $\theta = 20^\circ$ (red), and $\theta = 30^\circ$ (light blue). The principal curvature axes of the reflectors lie along the Cartesian coordinate axes. The size of each IFZ is normalized with respect to the incident P-wavelength for $\theta = 0^\circ$.

rays depend only on the vertical velocity of the medium and the results are the same as for isotropic media. Nevertheless, with increasing θ, the anisotropic IFZ shows significant changes in shape with respect to the isotropic counterpart. These changes are much more pronounced for positive values of $\epsilon - \delta$.

Figure 3 presents variations in the shape and size of the IFZ at an anticline-, syncline-, and saddle-type reflector, respectively, as a function of $\epsilon - \delta$ and for various incidence angles θ. The principal curvature axes of the reflectors lie along the Cartesian coordinate axes.

As expected in the case of an anticline, because a smaller area of the interface is in contact with the isochron, the anisotropic IFZ is smaller than that at the plane reflector. Whatever the value for $\epsilon - \delta$ and for small (or moderate) incidence angles, the size and the shape of the anisotropic IFZ are identical to the isotropic counterparts (Figure 3, top).

On the contrary, the anisotropic IFZ at the syncline-type reflector exhibits a more complex shape with increasing θ (Figure 3, middle). For small incidence angles, the IFZ has an elliptical shape with the major axis lying in the transverse plane, whatever the value for $\epsilon - \delta$. As the angle θ increases, the curvature of the isochron tends to that of the reflector over a very large distance, which leads to growing portions of the reflectors involved in the reflection process, and hence an unusually large IFZ in the incidence plane (e.g., for $\theta = 35^{\circ}$ in Figure 3 [middle]). Whatever the value for $\epsilon - \delta$, the size of the anisotropic IFZ at a syncline is larger than the isotropic counterpart. Nevertheless, this feature is still more pronounced for positive values of $\epsilon - \delta$. Note that for wider incidence angles the anisotropic IFZ exhibits four infinitely extended tails along diagonal directions, known as indicators of the existence of stationary points of hyperbolic type (Asatryan and Kravtsov, 1988; Spetzler and Snieder, 2004). Nevertheless, these tails are unphysical and must be truncated to obtain the actual field-formation region, which is of finite size (Asatryan and Kravtsov, 1988). The real size of the anisotropic IFZ is then given by the ellipse tangent to the vertices of hyperbolae and whose axes lie in the incidence and transverse planes.

The anisotropic IFZ at the saddle-type reflector exhibits a specific shape, which is a mix between the shapes of the anisotropic IFZ at the anticline and at the syncline (Figure 3, bottom). As expected from the values of the main radii of the interface curvature, its size is limited in the incidence (respectively, transverse) plane by the extent of the anisotropic IFZ at the syncline (respectively, anticline). The anisotropic IFZ at the saddle-type reflector is larger than the isotropic counterpart, this feature still being more pronounced for positive values of $\epsilon - \delta$.

Considering the general case in which the principal curvature axes of the reflectors do not lie along the Cartesian coordinate axes leads to significant changes in the shape and the size of the IFZ, more specifically for syncline- and saddle-type reflectors (Figure 4, middle and bottom). The IFZ patterns still remain ellipses expanding from the fixed reflection point with increasing incidence angle, but they are now rotated by the angle $\phi = 20^{\circ}$ with respect to the x_1-axis. In addition to the rotation of the patterns, the rotation of the principal curvature axes of the reflectors leads to larger (respectively, smaller) size of the isotropic and anisotropic IFZs at the syncline (respectively, saddle-type reflector) along the direction of the principal curvature axis associated with radius R_1, the size along the perpendicular direction remaining unchanged. Moreover, the occurrence of the infinitely extended tails along diagonal directions can be noted at the syncline for smaller incidence angles than previously. Finally, the anisotropic IFZs are larger than the isotropic counterparts, this feature still being more pronounced for positive values of $\epsilon - \delta$.

Influence of $\epsilon - \delta$ on the interface Fresnel zone for P-SV reflection from various curved reflectors

We now investigate the effects of the difference $\epsilon - \delta$ on the shape and the size of the IFZ for P-SV reflection for various incidence angles and various interface curvatures.

Figure 5 illustrates the results for a plane reflector. As noted in Eaton et al. (1991), the relative changes in size and shape of the isotropic IFZ for P-SV reflection for various incidence angles are not large and are comparable to the P-P reflection case. For $\theta = 0$, the anisotropic IFZ is equivalent to the isotropic counterpart and exhibits a circular shape. Nevertheless, with increasing θ, the anisotropic IFZ shows significant changes in shape and size with respect to the isotropic counterpart. For negative (respectively, positive) values of the difference $\epsilon - \delta$, the shape of the IFZ is almost circular (respectively, elliptical with the major axis in the incidence plane) and the center for the IFZ patterns is shifted left (respectively, right) of the reflection point for isotropic media. This peculiar property can be explained by examining the equations for the IFZ, as shown in Appendix C.

Figure 6 presents the variation in shape and size of the IFZ at an anticline-, syncline-, and saddle-type reflector, respectively, as a function of $\epsilon - \delta$ and for various incidence angles θ. The principal curvature axes of the reflectors lie along the Cartesian coordinate axes. For a fixed interface curvature, the isotropic IFZ has a symmetric shape centered at the reflection point and does not exhibit significant changes with increasing θ. On the contrary, the anisotropic IFZ exhibits significant variations in size and shape with increasing θ depending on the interface curvature. Its size is always much larger than the isotropic counterpart, this feature being much more pronounced for positive values of $\epsilon - \delta$. A shift of the center of the IFZ can still be noticed for negative and positive values of $\epsilon - \delta$.

Note that except the rotation of the patterns, the rotation of the principal curvature axes of the reflectors leads to no significant changes in the shape nor the size of the anisotropic IFZ.

CONCLUSIONS

The IFZ largely contributes to the formation of the reflection and transmission wavefields at an observation point. We have derived analytic expressions, based on traveltime approximations, to evaluate its size for converted and nonconverted waves reflected or transmitted by a curved reflector between two homogeneous anisotropic media. We have investigated the shape and size of the IFZ for P-P and P-SV reflections as a function of the anisotropy parameters for various incidence angles and interface curvatures. We have considered more specifically DTI media and reflectors of the anticline, syncline, and saddle type (with principal curvatures axes not necessarily lying along the Cartesian coordinate axes). In an anisotropic medium, the isochron in most cases assumes a nonelliptical shape. The size and shape of the IFZ for reflected waves are predominantly dependent on the curvatures of the isochrons together with the curvatures of the reflector. As expected, the syncline- and the

saddle-type reflectors exhibit very large IFZs compared to those for plane or anticline-type reflectors. In addition, the difference between the Thomsen anisotropy parameters ϵ and δ is found to also control the shape and size of the IFZ for P-P and P-SV reflections. The effects are much more pronounced for positive values of the difference $\epsilon - \delta$.

ACKNOWLEDGMENTS

Part of this work was done while B. Ursin was visiting the Laboratoire de Mécanique et d'Acoustique (LMA) in Marseille (France) in 2011. This work has received financial support from the Institute for Engineering and Systems Sciences (INSIS) of the French National Center for Scientific Research (CNRS) and from the Carnot STAR Institute (ICSTAR). B. Ursin has also received financial support from Statoil and from the Norwegian Research Council via the ROSE project. Anonymous reviewers, the associate editor M. van der Baan, and D. Komatitsch are greatly appreciated for their valuable suggestions that improved the paper.

APPENDIX A

GROUP VELOCITY

In a ray-tracing modeling scheme (e.g., Červený, 2001), the position vector $\mathbf{X}$ and the direction of the slowness vector $\mathbf{p}$ are known. The phase velocity C_I and the orthonormal polarization vectors $\hat{\mathbf{g}}_\mathbf{I}$ are determined from the Christoffel equation (e.g., Chapman, 2004):

$$(\hat{\mathbf{\Gamma}} - C_I^2)\,\hat{\mathbf{g}}_\mathbf{I} = \mathbf{0}, \tag{A-1}$$

where no summation over I is considered. The Christoffel matrix is

$$\hat{\Gamma_{ik}} = a_{ijkl}\hat{p}_j\,\hat{p}_l \quad (i,j,k,l = 1,2,3) \tag{A-2}$$

for an arbitrary slowness vector $\hat{\mathbf{p}}$, with $a_{ijkl} = c_{ijkl}/\rho$ being the density-normalized elastic moduli. Note that in equation A-2 the Einstein summation rule over repeated index has been used. The permitted slowness vector $\mathbf{p} = \hat{\mathbf{p}}/c_I$ satisfies

$$\det\,(\mathbf{\Gamma} - \mathbf{I}) = 0, \tag{A-3}$$

where $\mathbf{\Gamma}$ is given by equation A-2 with the slowness $\mathbf{p}$. With the help of the Hamiltonian defined by (e.g., Chapman, 2004)

$$H_I(\mathbf{X},\mathbf{p}) = \frac{1}{2}\hat{\mathbf{g}}_\mathbf{I}^t\mathbf{\Gamma}\hat{\mathbf{g}}_\mathbf{I}, \tag{A-4}$$

(with no summation over I) where the superscript t denotes the transpose of a quantity, the components of the group velocity vector are

$$V_i = \frac{\partial H}{\partial p_i} = \frac{1}{2}a_{ijkl}p_k\hat{g}_j\,\hat{g}_l\,. \tag{A-5}$$

Alternatively, the group velocity may be computed from the dispersion relation (Auld, 1990)

$$\Omega(\mathbf{K},\omega) = \det\,(\mathbf{\Gamma}(\mathbf{K}) - \omega^2\mathbf{I}) = 0 \tag{A-6}$$

with $\mathbf{K} = \omega\mathbf{p}$ (ω being the angular frequency), using

$$V_i = -\frac{\partial\Omega/\partial k_i}{\partial\Omega/\partial\omega}. \tag{A-7}$$

Zhou and Greenhalgh (2004) give a third method for computing the group velocities by taking derivatives of the phase velocities computed from equation A-1. Explicit expressions for group velocity through phase velocity can also be found in Tsvankin (2001).

APPENDIX B

GROUP VELOCITY COMPONENTS IN DIP-CONSTRAINED TRANSVERSELY ISOTROPIC MEDIUM

With $p_2 = 0$, the Christoffel equation reduces to (Chapman, 2004)

$$\begin{pmatrix} a_{11}p_1^2 + a_{44}p_3^2 - 1 & 0 & (a_{13}+a_{44})p_1p_3 \\ 0 & a_{66}p_1^2 + a_{44}p_3^2 - 1 & 0 \\ (a_{13}+a_{44})p_1p_3 & 0 & a_{44}p_1^2 + a_{33}p_3^2 - 1 \end{pmatrix}\hat{\mathbf{g}} = \mathbf{0}, \tag{B-1}$$

where $a_{ij} = c_{ij}/\rho$ are the density-normalized elastic constants, now in Voigt notation.

For the SH-wave, the Christoffel equation then gives (Chapman, 2004)

$$a_{66}p_1^2 + a_{44}p_3^2 = 1. \tag{B-2}$$

This equation leads to the expression for p_3 as a function of p_1:

$$p_3 = \pm\left(\frac{1}{a_{44}} - \frac{a_{66}}{a_{44}}p_1^2\right)^{1/2}. \tag{B-3}$$

From the dispersion equation A-6

$$\Omega(\mathbf{K},\omega) = a_{66}k_1^2 + a_{44}k_3^2 - \omega^2 = 0, \tag{B-4}$$

we obtain the group velocity components using equation A-7 additionally

$$\begin{cases} V_1 = a_{66}p_1 \\ V_3 = a_{44}p_3 \end{cases}. \tag{B-5}$$

For the coupled P-SV waves, the Christoffel equation B-1 gives (Chapman, 2004)

$$\begin{aligned}&(a_{11}p_1^2 + a_{44}p_3^2 - 1)(a_{44}p_1^2 + a_{33}p_3^2 - 1)\\ &\quad - (a_{13}+a_{44})^2p_1^2p_3^2 = 0.\end{aligned} \tag{B-6}$$

For a given horizontal slowness p_1, the solution for the vertical slowness is (Chapman, 2004)

$$p_3^2 = \frac{B \mp [B^2 - 4a_{33}a_{44}(a_{11}p_1^2 - 1)(a_{44}p_1^2 - 1)]^{1/2}}{2a_{33}a_{44}}, \tag{B-7}$$

with $B = a_{33} + a_{44} + (a_{13}^2 + 2a_{13}a_{44} - a_{11}a_{33})p_1^2$. In equation B-7, the minus sign is for the P-wave and the plus sign is for the SV-wave. The group velocity is computed from the dispersion relation:

$$\Omega(\mathbf{K},\omega) = (a_{11}k_1^2 + a_{44}k_3^2 - \omega^2)(a_{44}k_1^2 + a_{33}k_3^2 - \omega^2) - (a_{13} + a_{44})^2 k_1^2 k_3^2 = 0 \tag{B-8}$$

and using equation A-7,

$$\begin{cases} V_1 = p_1 \frac{a_{11}B_2 + a_{44}B_1 - p_3^2 A^2}{B_1 + B_2} \\ V_3 = p_3 \frac{a_{44}B_2 + a_{33}B_1 - p_1^2 A^2}{B_1 + B_2} \end{cases}, \tag{B-9}$$

with $B_1 = a_{11}p_1^2 + a_{44}p_3^2 - 1$ and $B_2 = a_{44}p_1^2 + a_{33}p_3^2 - 1$.

APPENDIX C

INTERFACE FRESNEL ZONE FOR A P-SV REFLECTION

We consider a P-to-SV-converted reflected wave in a DTI medium above a curved reflector. The IFZ is given by equation 15, where the absolute value sign can be removed because the quantity in the absolute value sign is positive due to Fermat's principle. The outer boundary of the IFZ can then be described using equation 16:

$$\frac{1}{2V_P d_P}\left(\frac{V_{P3}^2}{V_P^2}\delta x_1^2 + \delta x_2^2\right) + \frac{V_{P1}}{V_P^2}\delta x_1 + F(\delta x_1, \delta x_2)\frac{V_{P3}}{V_P^2} + \frac{1}{2V_S d_S}\left(\frac{V_{S3}^2}{V_S^2}\delta x_1^2 + \delta x_2^2\right) - \frac{V_{S1}}{V_S^2}\delta x_1 + F(\delta x_1, \delta x_2)\frac{V_{S3}}{V_S^2} = \frac{1}{2f}, \tag{C-1}$$

where the P (respectively, S) subscript is associated to the incident P-wave (respectively, the reflected SV-wave).

Because of the interface term $F(\delta x_1, \delta x_2)$, the IFZ is not necessarily symmetric about the x_1- and x_2-axes. Along the x_1-axis ($x_2 = 0$), the boundary of the IFZ is described by

$$a\delta x_1^2 + 2b\delta x_1 - \frac{1}{f} = 0 \tag{C-2}$$

with

$$a = \frac{V_{P3}^2}{V_P^3 d_P} + \frac{V_{S3}^2}{V_S^3 d_P} + F_{11}\left(\frac{V_{P3}}{V_P^2} + \frac{V_{S3}}{V_S^2}\right) \tag{C-3}$$

and

$$b = \frac{V_{P1}}{V_P^2} - \frac{V_{S1}}{V_S^2} \tag{C-4}$$

and whose solution is

$$\delta x_1 = \frac{1}{a}\left[-b \pm \left(b^2 + \frac{a}{f}\right)^{1/2}\right]. \tag{C-5}$$

When a is positive, there are two solutions of opposite sign. For $b < 0$, the positive solution is larger in absolute value than the negative one, whereas for $b > 0$, the negative solution is the largest one in absolute value. To analyze b in equation C-4, we use the approximate group velocities given in equations 22 and 23. This gives

$$b = p_1\left[(1 + 2\epsilon)\frac{v_{P0}^2}{V_P^2} - \frac{v_{S0}^2}{V_S^2}\right] - 2p_1(\epsilon - \delta)\chi v_{P0}^2\left(\frac{1}{V_P^2} + \frac{1}{V_S^2}\right). \tag{C-6}$$

From this expression, we note that b is large and positive when $\epsilon - \delta < 0$ and small, possibly negative, when $\epsilon - \delta > 0$. For $\epsilon - \delta = 0$, the sign of b depends on the V_P/V_S ratio. This explains the results in Figures 5 and 6, in which the IFZ lies mostly in the left half-plane ($\delta x_1 < 0$) when $\epsilon - \delta < 0$ and mostly in the right half-plane ($\delta x_1 > 0$) when $\epsilon - \delta > 0$.

REFERENCES

Alkhalifah, T., and I. Tsvankin, 1995, Velocity analysis for transversely isotropic media: Geophysics, **60**, 1550–1566, doi: 10.1190/1.1443888.

Asatryan, A., and Y. Kravtsov, 1988, Fresnel zones of hyperbolic type from the physical point of view: Wave Motion, **10**, 45–57, doi: 10.1016/0165-2125(88)90005-4.

Auld, B. A., 1990, Acoustic fields and waves in solids: Volume I, 2nd ed.: Wiley.

Ayzenberg, M., I. Tsvankin, A. M. Aizenberg, and B. Ursin, 2009, Effective reflection coefficients for curved interfaces in transversely isotropic media: Geophysics, **74**, no. 5, WB33–WB53, doi: 10.1190/1.3197862.

Červený, V., 2001, Seismic ray theory: Cambridge University Press.

Červený, V., and J. Soares, 1992, Fresnel volume ray-tracing: Geophysics, **57**, 902–915, doi: 10.1190/1.1443303.

Chapman, C., 2004, Fundamentals of seismic wave propagation: Cambridge University Press.

Eaton, D., R. Stewart, and M. Harrison, 1991, The Fresnel zone for P-SV waves: Geophysics, **56**, 360–364, doi: 10.1190/1.1443050.

Farra, V., and I. Pšenčík, 2013, Moveout approximations for P- and SV-waves in dipconstrained transversely isotropic media: Geophysics, **78**, no. 6, C53–C59, doi: 10.1190/geo2013-0083.1.

Favretto-Cristini, N., P. Cristini, and E. de Bazelaire, 2007a, Influence on the interface Fresnel zone on the reflected P-wave amplitude modelling: Geophysical Journal International, **171**, 841–846, doi: 10.1111/j.1365-246X.2007.03573.x.

Favretto-Cristini, N., P. Cristini, and E. de Bazelaire, 2007b, Some reflections on reflectors and wave amplitudes: Acta Acustica united with Acustica, **93**, 909–916.

Favretto-Cristini, N., P. Cristini, and E. de Bazelaire, 2009, What is a seismic reflector like?: Geophysics, **74**, no. 1, T13–T23, doi: 10.1190/1.3033216.

Gelchinsky, B., 1985, The formulae for the calculation of the Fresnel zones or volumes: Journal of Geophysics, **57**, 33–41.

Hubral, P., J. Schleicher, M. Tygel, and C. Hanitzch, 1993, Determination of Fresnel zones from traveltime measurements: Geophysics, **58**, 703–712, doi: 10.1190/1.1443454.

Iversen, E., 2004, The isochron ray in seismic modeling and imaging: Geophysics, **69**, 1053–1070, doi: 10.1190/1.1778248.

Iversen, E., 2006, Amplitude, Fresnel zone, and NMO velocity for PP and SS normal-incidence reflections: Geophysics, **71**, no. 2, W1–W14, doi: 10.1190/1.2187814.

Kravtsov, Y., and Y. Orlov, 1990, Geometrical optics of inhomogeneous media: Springer-Verlag, Series on Wave Phenomena.

Kvasnička, M., and V. Červený, 1994, Fresnel volumes and Fresnel zones in complex laterally varying structures: Journal of Seismic Exploration, **3**, 215–230.

Kvasnička, M., and V. Červený, 1996a, Analytical expressions for Fresnel volumes and interface Fresnel zones of seismic body waves. Part 1: Direct and unconverted reflected waves: Studia Geophysica et Geodaetica, **40**, 136–155, doi: 10.1007/BF02296354.

Kvasnička, M., and V. Červený, 1996b, Analytical expressions for Fresnel volumes and interface Fresnel zones of seismic body waves. Part 2: Transmitted and converted waves. Head waves: Studia Geophysica et Geodaetica, **40**, 381–397, doi: 10.1007/BF02300766.

Lindsey, J., 1989, The Fresnel zone and its interpretative significance: The Leading Edge, **8**, 33–39, doi: 10.1190/1.1439575.

Monk, D., 2010, Fresnel-zone binning: Fresnel-zone shape with offset and velocity function: Geophysics, **75**, no. 1, T9–T14, doi: 10.1190/1.3294576.

Moser, T. J., and V. Červený, 2007, Paraxial ray methods for anisotropic inhomogeneous media.: Geophysical Prospecting, **55**, 21–37, doi: 10.1111/j.1365-2478.2006.00611.x.

Okoye, P., and N. Uren, 2000, Fresnel zones and spatial resolution for P- and SH-waves in transversely isotropic media: Geophysics, **65**, 1168–1178, doi: 10.1190/1.1444810.

Pestana, R., B. Ursin, and P. Stoffa, 2012, Rapid expansion and pseudo spectral implementation for reverse time migration in VTI media: Journal of Geophysics and Engineering, **9**, 291–301, doi: 10.1088/1742-2132/9/3/291.

Pulliam, J., and R. Snieder, 1998, Ray perturbation theory, dynamic ray tracing and the determination of Fresnel zones: Geophysical Journal International, **135**, 463–469, doi: 10.1046/j.1365-246X.1998.00667.x.

Schleicher, J., P. Hubral, M. Tygel, and M. Jaya, 1997, Minimum apertures and Fresnel zones in migration and demigration: Geophysics, **62**, 183–194, doi: 10.1190/1.1444118.

Sheriff, R., 1980, Nomogram for Fresnel-zone calculation: Geophysics, **45**, 968–972, doi: 10.1190/1.1441101.

Spetzler, J., and R. Snieder, 2004, The Fresnel volume and transmitted waves — A tutorial: Geophysics, **69**, 653–663, doi: 10.1190/1.1759451.

Stavroudis, O., 1972, The optics of rays, wavefronts, and caustics: Academic Press.

Thomsen, L., 1986, Weak elastic anisotropy: Geophysics, **51**, 1954–1966, doi: 10.1190/1.1442051.

Tsvankin, I., 2001, Seismic signatures and analysis of reflection data in anisotropic media: Pergamon.

Tsvankin, I., and V. Grechka, 2011, Seismology of azimuthally anisotropic media and seismic fracture characterization: SEG.

Ursin, B., 1986, Zero-offset reflections from a curved interface: Geophysics, **51**, 50–53, doi: 10.1190/1.1442039.

Ursin, B., and A. Stovas, 2006, Traveltime approximations for a layered transversely isotropic medium: Geophysics, **71**, no. 2, D23–D33, doi: 10.1190/1.2187716.

Wang, Z., 2002, Seismic anisotropy in sedimentary rocks, Part 2: Laboratory data: Geophysics, **67**, 1423–1440, doi: 10.1190/1.1512743.

Zhou, B., and S. Greenhalgh, 2004, On the computation of elastic wave group velocities for a general anisotropic medium: Journal of Geophysical Engineering, **1**, 205–215, doi: 10.1088/1742-2132/1/3/005.